Finite Element Modelling of the Effect of Temperature and Neutron Dose on the Fracture Behaviour of Nuclear Reactor Graphite Bricks

M. Wadsworth, S.T. Kyaw*, W. Sun

Faculty of Engineering, The University of Nottingham
University Park, Nottingham, NG7 2RD, UK

***Corresponding authour email: si.kyaw@nottingham.ac.uk**
Address: C03, ITRC building, University Park, University of Nottingham, NG7 2RD
Phone: +44-1159513811

Abstract

Graphite moderator bricks used within many UK gas-cooled nuclear reactors undergo harsh temperature and radiation gradients. They cause changes in material properties of graphite over extended periods of time. Consequently, models have been developed in order to understand and predict the complex stresses formed within the brick by these processes. In this paper the effect of irradiation temperature and neutron dose on the fracture characteristics, crack initiation and crack growth are investigated. A finite element (FE) mechanical constitutive model is implemented in combination with the damage model to simulate crack growth within the graphite brick. The damage model is based on a linear traction-separation cohesive model in conjunction with the extended finite element method for arbitrary crack initiation and propagation. Results obtained have showed that cracks initiate in the vicinity of the keyway fillet of the graphite brick and initiation time accelerates with higher temperatures and doses.

Keywords

Nuclear graphite, neutron dose, irradiation temperature, crack growth, cohesive damage

1. INTRODUCTION

UK advanced gas-cooled nuclear reactors (AGRs) rely upon graphite bricks as a method of moderating the speed of fast neutrons in order to maintain a nuclear reaction in addition to performing a structural role in the reactor. Graphite bricks are interconnected using keys and keyways to form structures that allow for the movement of control rods and the loading and unloading of fuel [1]. These bricks undergo loading, from both radiation and high temperatures,

as a direct result of the fission reaction. Thermal stresses can be developed from temperature loading and additional stresses can be developed within the graphite brick due to material properties changes because of irradiation. Moreover, stresses can also be developed from dimensional changes in graphite crystal and irradiation induced creep can cause relaxation in stresses. Currently, a total of 14 AGR reactors operate in the UK at an average core temperature of 538°C. Higher temperatures and neutron doses are expected for future generation of nuclear reactors for higher efficiency. To perform structural integrity assessment on graphite bricks, the complex stress field due to different loading conditions need to be understood. In this paper, parametric studies of temperature and dose on fracture behaviour of graphite bricks are carried out using a finite element method.

A finite element (FE) approach is developed based on the hypothetical brick model developed by Tsang and Marsden [1] with a user defined material model. Without any mechanical loads, the material model derives a stress/strain constitutive relationship based on different physical mechanisms within graphite bricks. These mechanisms include dimensional changes caused by irradiation, porosity change as a result of oxidation and microstructure changes from fast neutron damage. To adapt this model further to study fracture behaviour of the bricks, a traction-separation cohesive surface model, in conjunction with the extended finite element method (XFEM) is applied within ABAQUS. This particular model has been developed for a near isotropic form of graphite known as Gilsocarbon, primarily developed for use in the AGRs.

2. Graphite Brick Model

2.1. Geometry and boundary conditions

The graphite brick model is based on a hypothetical brick design and the exact dimensions of the brick can be seen in Fig. 1 (a) with the keyway radius of 6mm. Only one-eighth of the brick geometry shown in Fig. 1 (a) was used with the aim of saving computation time. In order to achieve this, symmetry and periodic boundary conditions are applied to the nodes along B1 and B2 respectively (Fig. **1** (a)). However, the circumferential degree of freedom displacements for periodic boundary conditions are transformed into rectangular ones by using a 45 degree transformation [2]. This is because ABAQUS displacement degree of freedom is based on a rectangular coordinate system. Finally displacements of nodes along B1 and B2 for symmetric and periodic boundary conditions are shown in Eq (1) and Eq (2) respectively.

$$u_X = 0 \text{ , along B1} \tag{1}$$

$$u_\theta = 0 \rightarrow -u_X \cdot \sin\theta + u_Y \cdot \cos\theta = 0 \text{ , along B2} \tag{2}$$

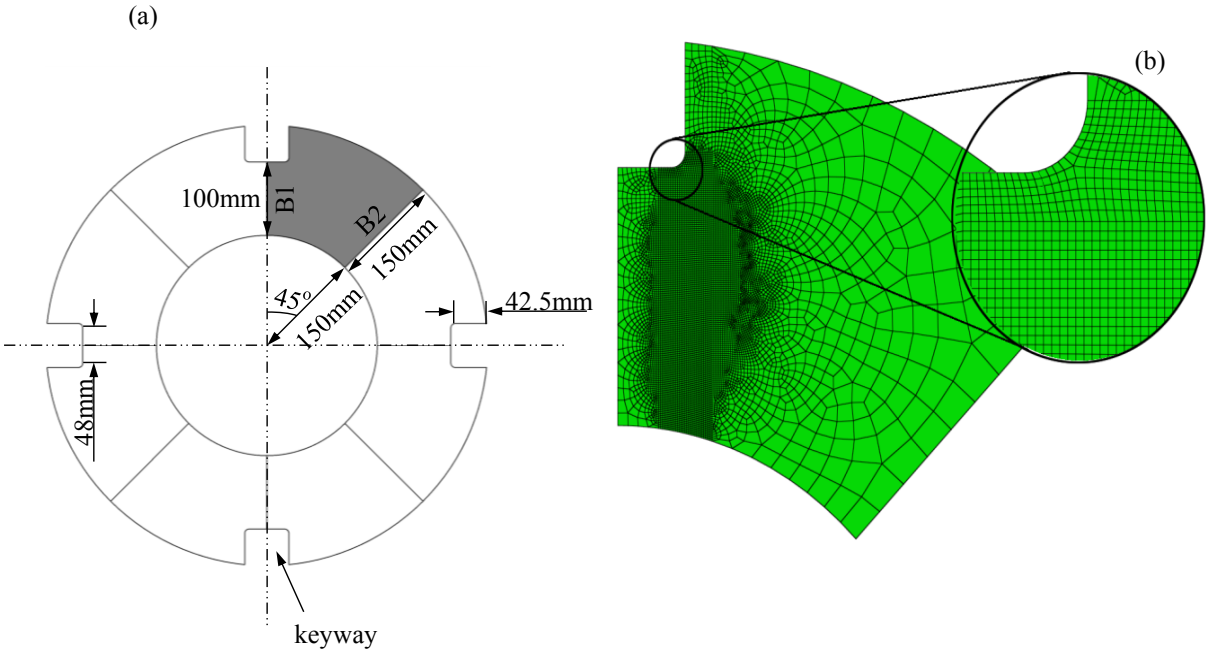

Fig. 1: (a) Full Graphite brick geometry, with one-eighth brick highlighted in grey is used for FE model (b) FE mesh of graphite brick showing the detail of mesh structure around the 6mm fillet radius

2.2. FE Mesh

Commercial FE software Abaqus 6.11 [3] is used for FE analysis of the current study and Fig. **1** (b) shows the mesh structure of a brick model. The elements used are 4-node bilinear plane strain quadrilateral elements (CPE4) under the assumptions that the length of the brick is much larger than other geometries and no variations exist in the material properties along the axial direction. The mesh is required to be suitably refined in regions of high displacement gradients so that stresses and resultant crack propagation by XFEM are accurately predicted. Although XFEM is a mesh-independent method, it does not allow the crack tip to reside within an element and it must terminate at an element boundary. This is because the XFEM enrichment does not utilise a crack tip enrichment function. It is expected from previous analyses by Kyaw et al. [4] that the highest maximum principal stresses will develop within the 6mm fillet radius of the keyway. The initiation of cracks also most likely to occur at the same region as cracks

are assumed to initiate perpendicular to the maximum principal stress and then continue propagating toward the inner edge of the brick. The elements in this area are quad-structured square elements with an approximate size of 0.8mm. Surrounding this region, elements have larger sizes as the resolution of stresses is less important.

2.3. Loading conditions

The FE model is set to simulate 30 years of plant operation. No mechanical loading is implemented within the model. Operating and irradiation temperatures, neutron fluence and weight loss, which resemble the plant operation conditions, are implemented at nodal points of the model using predefined field variables within ABAQUS input files. The operating temperature is constant throughout the simulation of the steady state while it varies linearly across the radius of the brick. Regardless of the reactor core temperature, the temperature difference from the inner to the outer edge of the brick is 100°C. Throughout the simulation, irradiation temperature is identical to the operating temperature but the operation temperature is ramped down to 20°C at the end of 30 years while the irradiation temperature is kept constant. Comparatively, the fluence dose is ramped upwards from zero at the beginning of the reactor life. At the end of operation the fluence dose varies quadratically across the brick from $214x10^{20}$ n/cm^2 at the inner radius to $106x10^{20}$n/cm^2 at the exterior. The neutron dose is expressed in terms of equivalent DIDO nickel dose (EDND) which is calculated so that the damage rate experienced by the graphite at a given location is equivalent to that of graphite test samples irradiated in the DIDO reactor [5]. Due to the fact that the empirical linear relationship between weight loss and the radiation dose from [6] is applied here, weight loss also varies quadratically across the radius of the brick.

2.4. Graphite Properties

Gilsocarbon graphite is manufactured by mixing naturally occurring filler known as Gilsonite, with coal-tar pitch binder. It is then moulded to shape and baked at 1000°C and impregnated with pitch. Following this it is baked for a second instance at 2800°C to graphitize the material [7]. The typical virgin material properties of this particular graphite are shown in Table 1.

Table 1: Typical properties for virgin isotropic Gilsocarbon graphite [1]

Material Property of Isotropic Graphite	Values
Density	1.81g/cm^3
Mean Coefficient of Thermal Expansion (CTE)	4.35x10^{-6} (°C)$^{-1}$
Poisson's Ratio	0.2
Dynamic Young's Modulus	10GPa

The properties of graphite vary once subjected to the high speed neutrons leaving the reactor core which collide with its own moderator atoms. These collisions result in atomic displacement causing material defects such as interstitial loops and lattice vacancies. These defects with increasing fluence cause changes in material properties of graphite (Young's modulus, irradiation creep and CTE). Virgin graphite includes porosity, caused by shrinkage during manufacture in addition to inter-crystalline cracks, known as Mrozowski cracks [8]. Gas evolution during graphitisation also creates porosity. The porosity volume is further increased during operation under irradiation due to radiolytic oxidation. Consequently, weight loss within the material and an eventual reduction in strength occur [9]. Dependence of weight loss due to thermal oxidation is not considered here.

In order to simulate crack growth within graphite brick, tensile strength and critical strain energy release rate (G) are required. For virgin graphite, tensile strength of 22.3 MPa is taken from [10]. It is assumed that the evolution of tensile strength due to weight loss from radiolytic oxidation is similar to the trend of flexural strength given in [11]. The values of tensile strength at different doses are tabulated in Table 2. Early increase in strength might have been the result of hardening caused by neutron radiation. However, overall decrease in tensile strength is observed as the dose level is higher than 5×10^{20} n/cm^2. Empirical data of critical strain energy release rate (G) due to weight loss from radiolytic oxidation is not available in the literature. Hence, it is assumed that G is independent on irradiation and changes in G due to oxidation data from [12] are applied here. The crack is assumed to initiate when the maximum principal stress exceeds the tensile strength whereas propagation of crack occurs once the energy release rate exceeds the critical value. The direction of crack is perpendicular to the direction of the maximum principal stress. More detail of the model for simulating crack growth is described in Section 4. Material properties used for the current work are for Gilsocarbon graphite used in

older generations of nuclear reactors with carbon dioxide coolant where radiolytic oxidation is important. Relevant adjustments to the material data in [1] are still required for future generation reactors with other type of coolant for which radiolytic oxidation is of less importance.

Table 2: Tensile strength values of graphite at different dose value

Dose ($\times 10^{20}$ n/cm^2)	Tensile strength (MPa)
0	22.2
5	42.6
10	36.6
15	31.0
20	26.0
30	17.9
35	14.8

3. Stress Analysis Code

The model to describe the behaviour of graphite brick under nuclear reactor conditions is implemented using ABAQUS' user material subroutine (UMAT). An overview of the FE model can be seen in Fig. 2. The model requires the input of four field operating variables for loading conditions: the operating and irradiation temperatures, neutron fluence and weight loss. Initially ABAQUS estimates the total strain within the model at the beginning of each increment. Using the total estimated strains UMAT decomposes the total strain into strain related to different physical processes. After strain decomposition, UMAT calculates the total stresses and updates them at the end of the increment. UMAT also provides the Jacobin matrix $\left(\frac{\partial \Delta\sigma_{ij}}{\partial \Delta\varepsilon_{ij}}\right)$ for the changes in stress ($\Delta\sigma_{ij}$) and strain ($\Delta\varepsilon_{ij}$) at the end of each time increment to help with convergence of solution. The stresses are then input into Abaqus FE code and they are also used by the linear damage model to predict initiation and propagation of cracks. The damage model will be discussed in detail in the subsequent section.

The total strain(ε^T) for the current problem as shown in Eq (3) is made up of seven strain components: ε^e, the elastic strain, ε^{pc}, the primary creep strain, ε^{sc}, the secondary creep strain, ε^{dc}, the dimensional change strain induced by irradiation, ε^{th}, the thermal strain, ε^{ith}, the interaction thermal strain and ε^{idc}, the interaction dimensional change strain. The elastic strain is a standard function of Hooke's law of linear elasticity. The creep caused by irradiation can

be split into two stages; the first is a primary transient creep strain which is recoverable. It causes rapid deformation which gradually reduces with increasing irradiation fluence. Following this the secondary creep strain takes place which is an unrecoverable, steady state creep strain. These two creep strains are irradiation induced creep strains and they are assumed to be independent of temperature. The creep model used is UKAEA model by Kelly and Brocklehurst [13]. The dimensional change strain is assumed to be dependent on the irradiation fluence, temperature and weight loss. The interaction thermal strain and interaction dimensional change strain are assumed to be functions of irradiation creep in graphite. These strains are proposed by Kelly and Burchell [14] as a correction factor to accommodate the changes made by total creep strain on CTE of graphite and dimensional change strain. More detailed explanations can be found in [15]. A complex stress field is created due to the discrepancy of various stresses created by these different strains.

$$\varepsilon^{T} = \varepsilon^{e} + \varepsilon^{pc} + \varepsilon^{sc} + \varepsilon^{dc} + \varepsilon^{th} + \varepsilon^{ith} + \varepsilon^{idc} \tag{3}$$

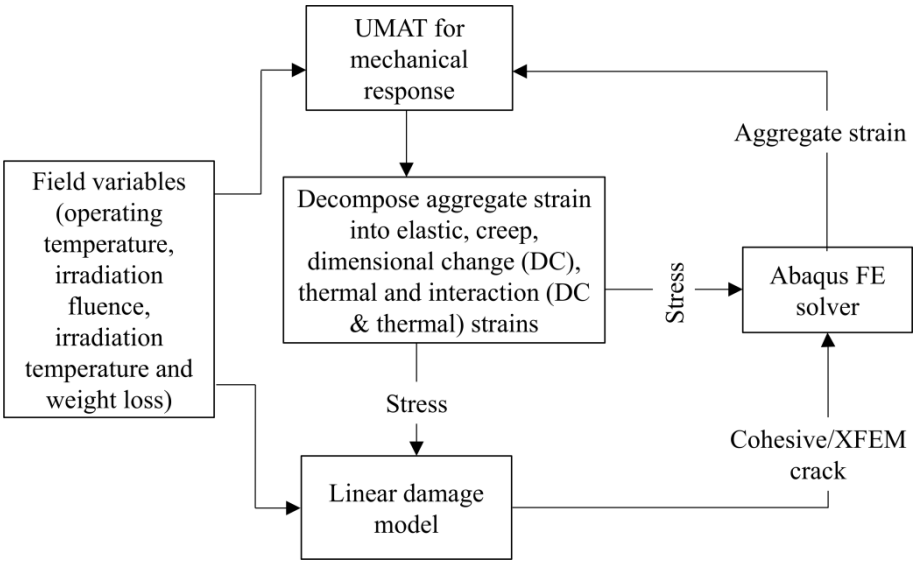

Fig. 2: Flowchart demonstrating FE model including UMAT and fracture damage model

4. Methodology for Fracture Mechanics Based Damage Model

To model the propagation of cracks within graphite bricks, cohesive traction-separation damage model is applied. The model is phenomenological and it combines complex damage

mechanisms around the crack tip into a single cohesive zone without implicitly modelling them using complex multi-scale approach. The resistance energy of crack growth due to different damage mechanisms within a cohesive zone can be related to empirical fracture toughness. The approach has been used by other researchers [16, 17] for fracture analysis of nuclear graphite. Traction stresses (T) across this cohesive zone can be associated with the crack separation (δ), for a linear damage model, as illustrated in Fig. 3. As traction increases towards its peak value the separation between crack faces (δ) increases. Before point X, the crack interface is elastic and upon unloading the separation goes back to zero. Different criteria can be applied to describe the damage initiation at point X. For e.g. maximum nominal stress or strain, maximum principal stress or strain can be used for mode I fracture and quadratic criteria are used for mixed mode failures. Nominal stress or strain criterion is suitable for uniaxial tests since the crack initiation depends on a single component of stress or strain. In this study, the maximum principal stress criterion is used to consider every components of stress that leads to crack initiation. Damage initiates when the maximum principal stress exceeds the material strength; in this case the tensile strength of the material. Only mode I failure is considered due to lack of experimental data for mixed mode fracture of irradiated graphite.

Being a quasi-brittle material, graphite does not fail instantly at critical traction and it shows strain softening behaviour as a result of micro-cracking and grain bridging near the crack tip. This is demonstrated by the line XZ in Fig. 3. Work is in progress [18] for the usage of more sophisticated model such as trilinear cohesive model to accurately represent the effect of micro-cracking and grain bridging on overall fracture toughness of graphite. Currently, a linear model shown in Fig. 3 is used. The gradient of the line OX (K) represents the cohesive stiffness of an undamaged material. Once the crack initiates the stiffness reduces to K(1-D). Damage parameter (D) is set so that D=0 and D=1 represent zero damage at point O and a fully cracked condition at point Z respectively. It can be proved that D at point Y (Fig. 3), can be linked to maximum crack separation (δ_z), separation at maximum traction stress ($\underline{\delta}$), and at the unloading point Y (δ_Y) as shown in Eq (4). The critical crack length opening is described in terms of the fracture stress ($\underline{T}$) and the fracture toughness (K_c) by Eq (5). The area underneath a triangle OXZ (Fig. 3) describes the critical strain energy release rate and cohesive zone is completely damaged the crack tip propagate further.

$$D = \frac{\delta_z(\delta_y - \underline{\delta})}{\delta_y(\delta z - \underline{\delta})} \tag{4}$$

$$\delta_z = \frac{2K_C^2}{E\underline{T}} \tag{5}$$

A conventional cohesive model is a simple way to model crack propagation but it requires a priori crack path. To avoid this restriction, XFEM is used in combination with traction-separation cohesive model. The XFEM method is an extension of the conventional finite element method which is based on the partition of unity finite element method (PUFEM) developed by Melenk and Babuska [19]. Using a displacement interpolation scheme shown in Eq (6) it allows for the presence of discontinuities in an element by enriching the degrees of freedom with displacement functions. The direction of the crack path is dependent on crack initiation criterion used for cohesive model and the crack propagates perpendicularly to the direction of the principal stress for the current study.

$$u^h(x) = \sum_{I \in N} N_I(x) \left[u_I + \underbrace{H(x) a_I}_{I \in N_\Gamma} + \underbrace{\sum_{\alpha=1}^{4} F_a(x) b_I^\alpha}_{I \in N_\Lambda} \right] \tag{6}$$

where u^h is the displacement vector and N_I represents the shape functions used for elements which are the same regardless of whether the XFEM enrichments are used. u_I are the nodal displacement vectors for conventional shape functions N_I, while $H(x)$ is the Heaviside enrichment for the jump discontinuity between the crack faces. $F_\alpha(x)$ is the crack tip asymptotic function which along with b_I^α, the nodal enriched degree of freedom vector, makes up the crack tip enrichment term [3].

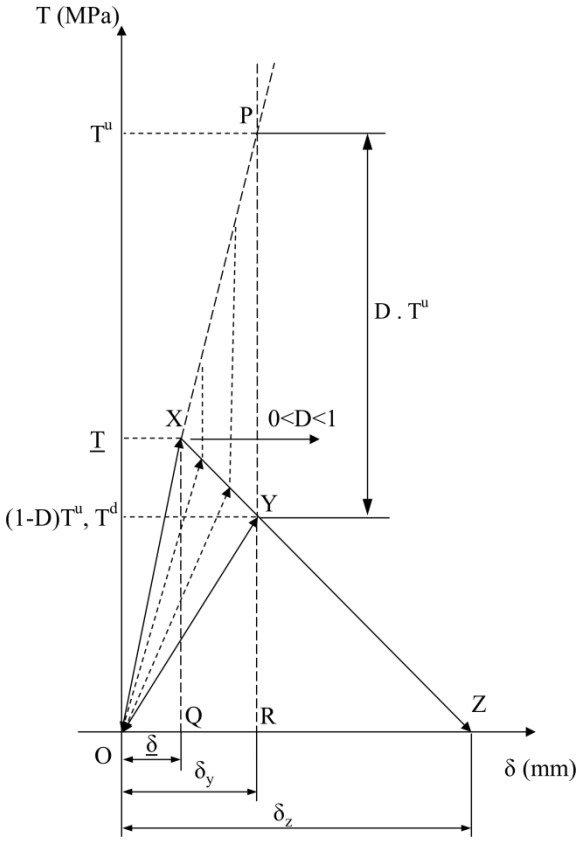

Fig. 3: Linear traction-separation cohesive model [4]

5. Results and discussion

5.1. Effects of temperature on fracture characteristics of graphite bricks

The effect of temperature on graphite brick failure is important since future generation reactors are expected to operate at temperatures much higher than the limit of current reactors for higher efficiency. Due to limited availability of irradiated properties of graphite to be used in future generation of reactors, the temperature dependent properties used within the current work is based on the properties from [1]. Four parametric FE analyses were carried out using various temperatures. Irradiation time is 30 full power years for all simulations. The temperature range varies from 500°C to 750°C while the maximum dose level remains constant for each simulation. Weight loss is assumed to be temperature independent although this area needs further studies due to possible effects of thermal oxidation at higher temperature and subsequent weight loss, in addition to radiolytic oxidation.

Regardless of the operating temperature, it is observed that a crack initiates in the vicinity of the fillet keyway radius. The crack then propagates for a short distance (4.37mm) at approximately 10° angle from the radial direction. Once the crack achieves this length its

direction changes, so that the fracture path traces a straight line approximately along the radius of the brick, suggesting that the maximum principal stress acts in the hoop direction apart from the area in the vicinity of the fillet region. Fig. 4 shows the typical crack geometry within the brick at the end of operation at 500˚C. The final distinct region of crack propagation is a wavy segment showing unstable crack propagation region but the changes in crack direction is insignificant and generally the crack can be assumed to be perpendicular to the hoop direction of the brick.

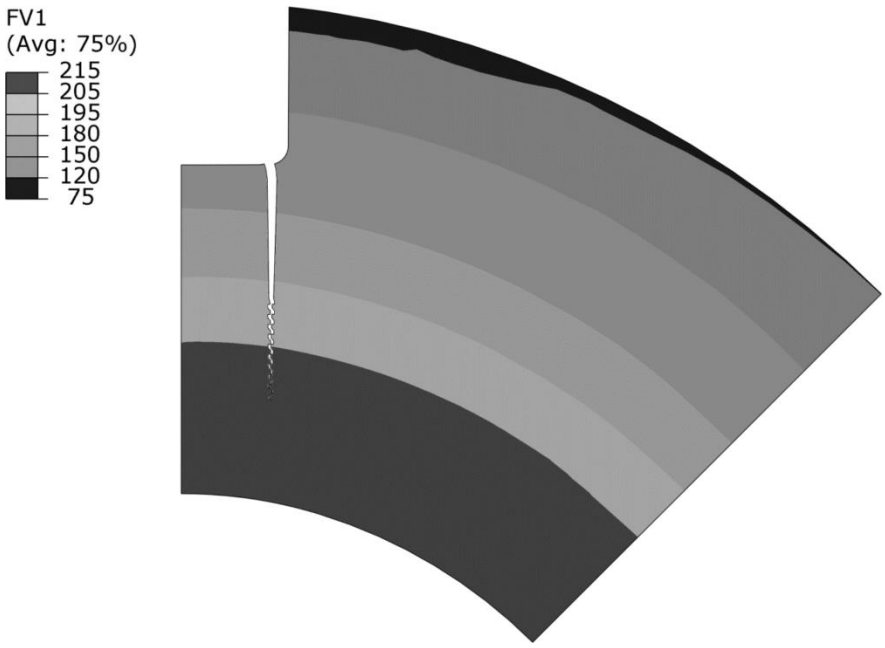

Fig. 4: Visualization of the graphite brick after 30 year of operation with crack (showing contours of neutron dose ($\times 10^{20}$ n/cm^2) at 500˚C)

Fig. 5 shows the effect of temperature on crack initiation time and time to reach the maximum crack length. Crack initiates faster at higher temperatures. Maximum principal stresses (used as a crack initiation criterion for XFEM analysis) at the crack initiation site for different operating temperatures are plotted against the operating time in Fig. 6. As shown in the figure, for every temperature, there is a region with a sharp increase in maximum principal stresses before a sharp decline in stresses due to relaxation by crack initiation. To illustrate the cause of sharp increase in maximum principal stresses, stresses and strain at the crack initiation site of the crack free model (without cracks) at 500˚C are plotted in Fig. 7. It shows that both radial and hoop strains are decreasing with the operating time but there is a turnaround point where the hoop strain increases significantly with the increase of time. Maximum principal

stress which leads to crack initiation is also increased at this point where sudden change in hoop strain occurs. The same turnaround point in hoop strain can be observed for all temperatures as plotted in Fig. 8. Turnaround point also occurs earlier as the temperature is increased and hence crack initiation which occurs at the same turnaround point becomes quicker too. The trend can be seen from Fig. 5. Nevertheless, further study is needed to identify the component of strain shown in Eq (3) which causes the turnaround behaviour in the hoop strain.

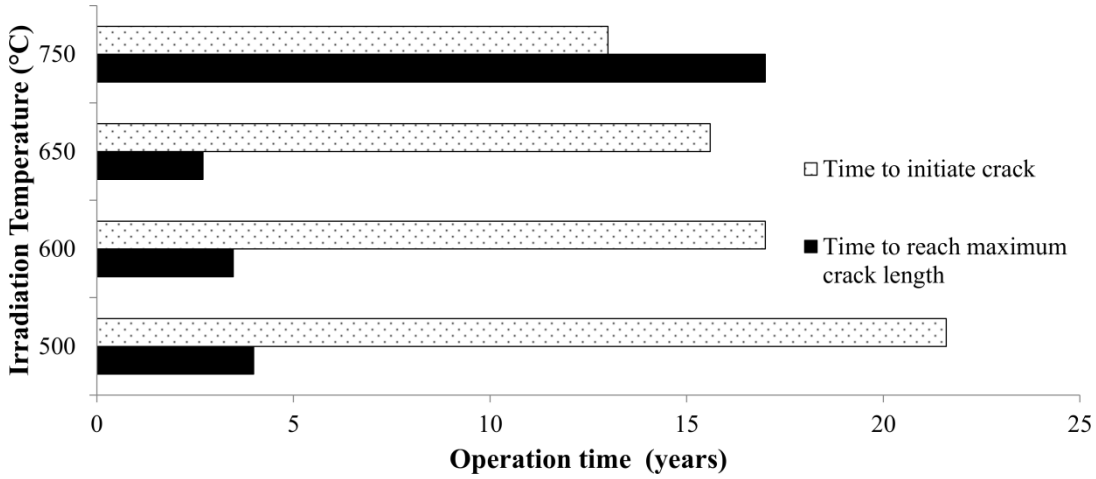

Fig. 5: Effect of irradiation temperature and operation time on crack initiation time and on time to reach maximum crack length

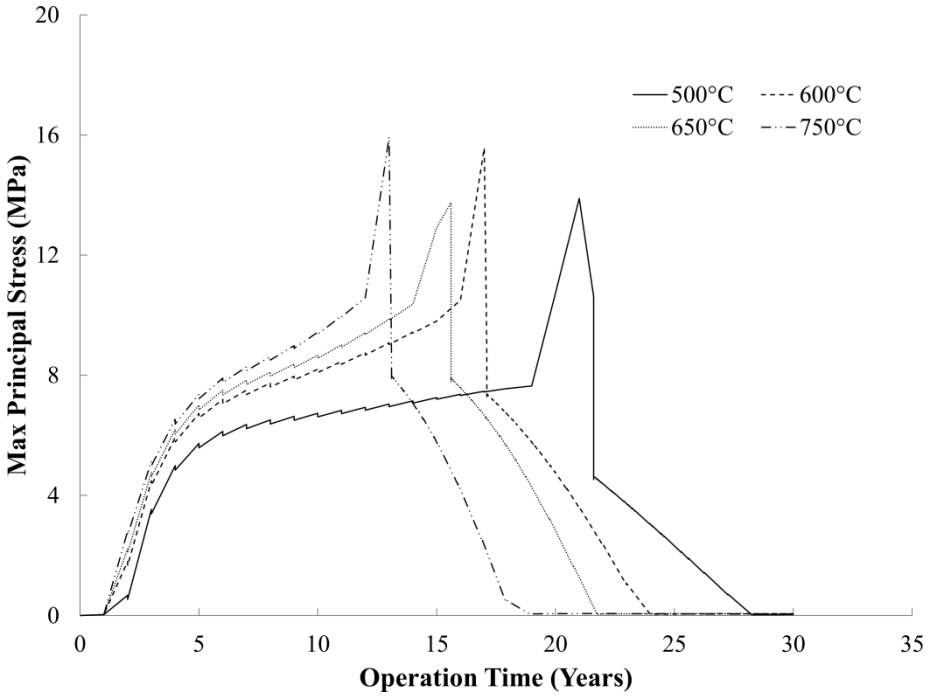

Fig. 6: Maximum Principal Stress plotted against the operation time at the keyway radius where crack initiates for various operating temperatures

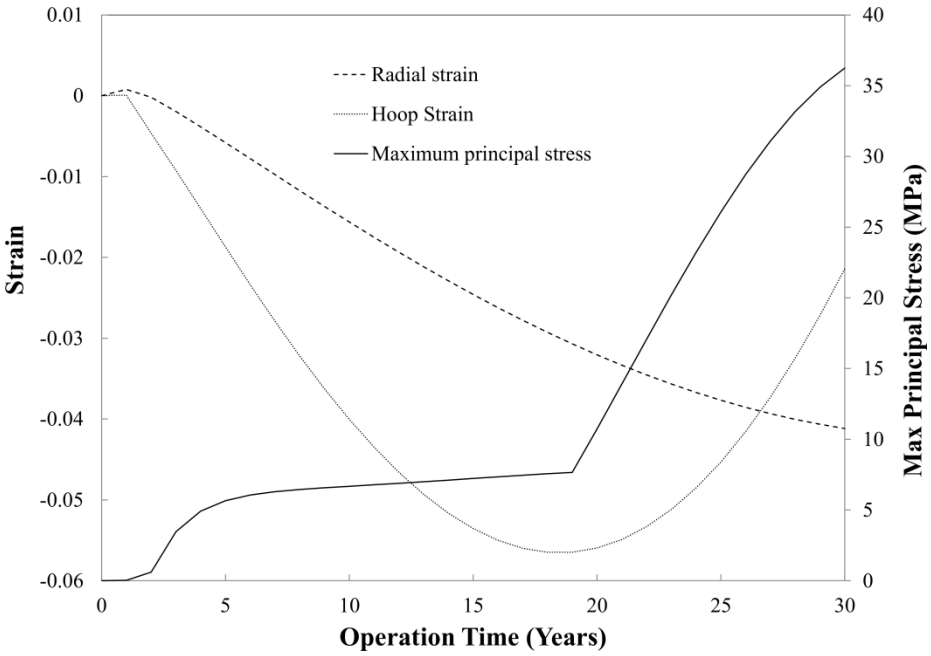

Fig. 7: Maximum principle stress, hoop and radial strains at the crack initiation point of keyway fillet at 500˚C (without damage or crack within the model)

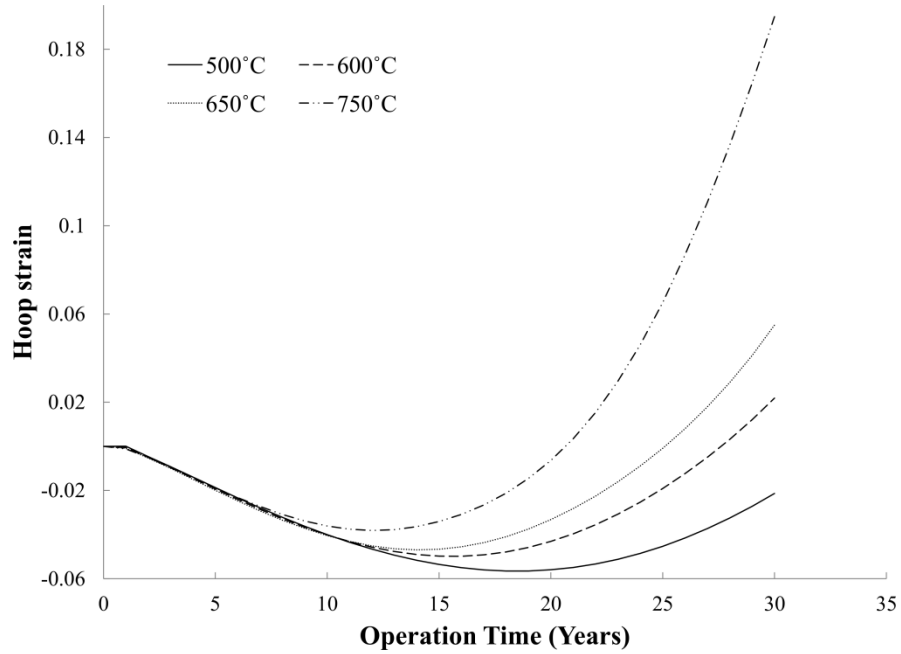

Fig. 8: Hoop strain at the crack initiation point of keyway fillet for different temperatures (without damage or crack within the model)

At higher irradiation temperatures both the rates of changes in hoop strain and the changes in the maximum principal stresses are increased as shown in Fig. 6 and Fig. 8 respectively. Hence cracks are expected to propagate faster as temperature is increased. However, this trend is interrupted at 750°C for which a crack takes 17 years until it stops propagating as shown in Fig. 5. Analysing further for this case, it was found that it takes approximately 37 days for the final crack to reach 82% of its final length and the crack grows faster than other models with lower temperatures during this period. Hence significant slowing down of crack growth occurs around this time and it can be explained by a rapid decline in CTE as the crack tip reaches a region of high neutron dose. The decline in growth rate of the crack is evident for all irradiation temperatures, but has the largest effect on the 750°C simulation. Tsang and Marsden [15] have shown that increasing dose leads to a steep decline in CTE for the temperature range between 350°C and 550°C. The data also shows that the higher the temperature is the steeper the decline in CTE becomes. Therefore extrapolating this data to a temperature of 750°C, the CTE and respective thermal strain will be heavily reduced, lowering overall stress level and subsequently slowing down the crack initiation significantly.

At the end of operation for 30 years, CTE of graphite varies across the graphite brick due to variation in dose and temperature loads during operation. Hence, thermal mismatch stresses are expected when the brick is cooled down to 20˚C at the end of operation. For example, the evolution of maximum principal stress due to mismatch for 500˚C case is illustrated in Fig. 9. Noticeably, the stress level at the outermost part of the brick has increased significantly after the brick has cooled down to 20˚C as shown in Fig. 9 (b). The stress level is below the fracture strength of the graphite after 30 years of operation. The trend is similar for other cases with different operating temperatures. As a result, initiation of new cracks during cooling down stage is expected at the outermost region of the aging bricks with high weight loss level. This is because the graphite strength, as demonstrated in [11], is reduced significantly as the weight loss increases.

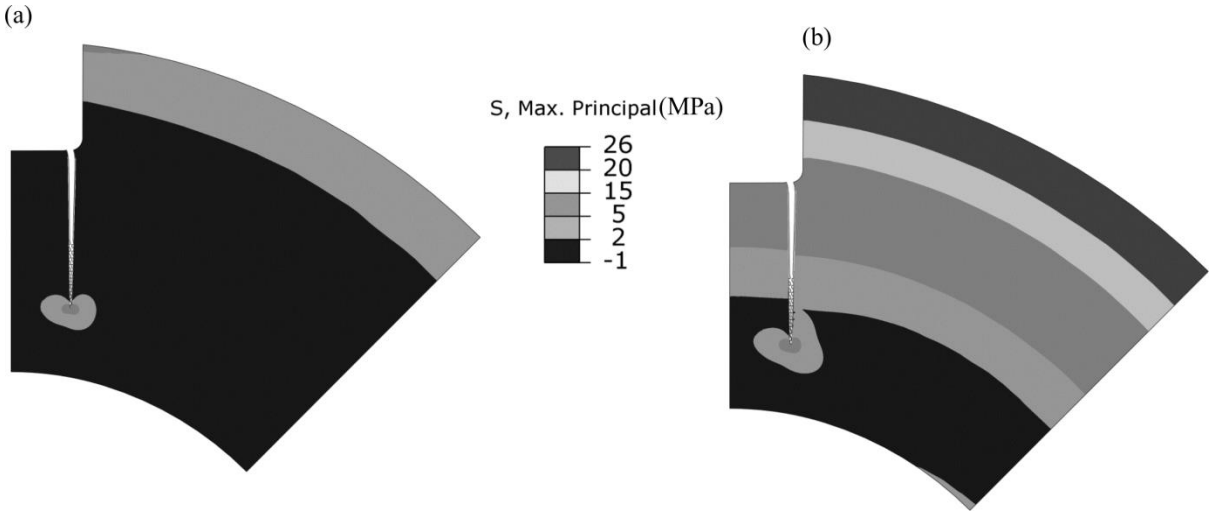

Fig. 9: Maximum principal stress state within the brick after 30 year of operation at 500˚C (a) before cooling down (b) after cooling down to 20˚C

5.2. Effects of neutron dose on fracture characteristics of graphite bricks

Simulations with 5% and 10% above and below of the baseline dose distribution from Section 2.3 were performed at constant temperature of 500°C. The weight loss as a function of the dose was also varied. One of the most noticeable results from this study is the change in direction of the cracks at dose levels above 5% and 10% of the baseline dose as illustrated in Fig. 10. The direction of cracks change and they propagate along the hoop direction for approximately 7.71mm, before returning to the radial direction. However, additional experimental data is required to confirm this behaviour of crack growth. This stage of growth

also demonstrates slower growth rates. Cracks grow in hoop direction for approximately 0.59 and 0.57 years for the cases with doses 5% and 10 % above baseline dose respectively. Conversely, the 5% below simulation takes approximately 3.2 days to grow around 80% of the total crack length.

Since hoop strain turnaround occurs at the same dose for a given temperature in this study, increasing the final dose level reduces the crack initiation time as shown in Fig. 10. As dose rises by 5% each time, the fracture initiation time decreases by approximately 5%. Due to decline in CTE and thermal strain at higher doses as explained in the previous section, crack propagate less as the dose is increased. Distances of crack tips from keyway fillet at different levels of doses are tabulated in Table 3.

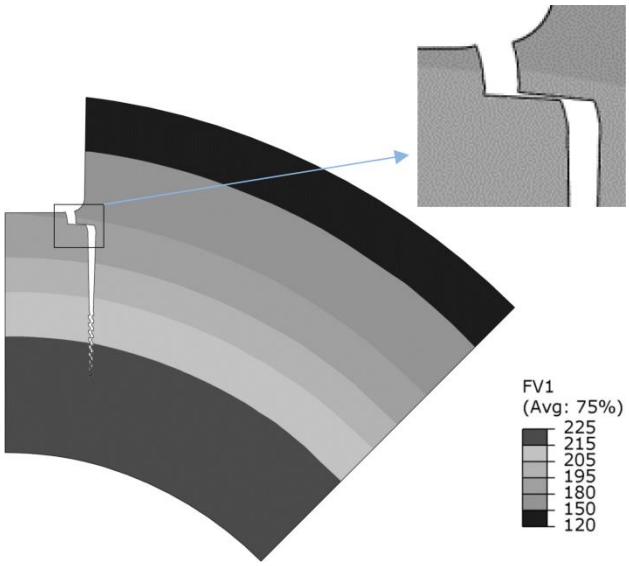

Fig. 10: Illustration of propagation of the crack along the hoop direction for the case with dose 5% above the baseline distribution at an operation temperature of 500°C (contours of neutron dose (× 10^{20} n/cm^2))

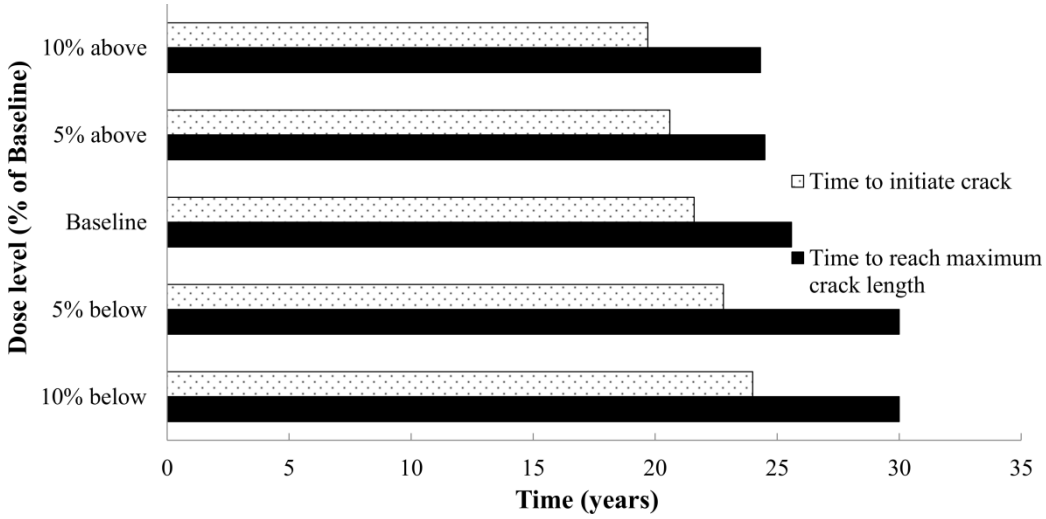

Fig. 11: Effect of neutron dose and operation time on crack initiation time and on time to reach maximum crack length

Table 3: Length of crack in the radial direction for each dose value

Dose	Distance of crack tip from the keyway fillet (mm)
10% above the original level	70.24
5% above the original level	70.1
Baseline dose level	70.82
5% below the original level	72.92
10% below the original level	74.34

6. Conclusions and future work

In this paper parametric studies to analyse the influence of irradiation temperature and neutron dose on the characteristics of crack propagation in Gilsocarbon nuclear graphite bricks are presented. The study is particularly useful in understanding the failure of graphite bricks under operating conditions of the current and future generation reactors. By using a constitutive stress analysis code in conjunction with a cohesive linear damage model and XFEM, arbitrary crack propagation was predicted with maximum principal stress which was used as the main fracture criterion.

During the temperature study it was found that turnaround time of hoop strain coincides with crack initiation time for each temperature condition. It is currently assumed that this turnaround in hoop strain is driven by turnaround behaviour of dimensional change strain but further studies are needed in this area. The turnaround time, and thus fracture initiation time

are significantly dependent upon irradiation temperature; lower irradiation temperatures delayed the onset of fracture dramatically, whereas higher irradiation temperatures caused an increase in the rates of shrinkage and expansion. A decrease in the rate of crack propagation was seen once the crack had grown to around 80% of its total length, which was caused by a decrease in the CTE as a result of the crack tip entering regions of higher neutron dose. Similarly to the temperature study, crack initiation within nuclear graphite brick speeds up as dose increases. This is because the turnaround occurs at the same dose for a given temperature; hence crack initiation will vary by the same degree as dose when irradiation levels are changed.

When the data for mixed mode fracture properties of nuclear graphite are available in the future, the current studies based on 2D FE analyses will be extended to 3D analysis. This would reveal the crack initiation sites along the axial direction by using mixed mode failure criteria for damage model. Causes of turnaround in hoop strain need to be investigated further and this can eventually be used an estimation factor for crack initiation within graphite bricks. Future generation reactors operating conditions can also be tested with new geometries as well as an updated mechanical behaviour model that is viable for temperatures up to 1000°C. For instance, thermal creep of graphite, which is not considered in the current model, will be important for future generation reactors. Due to higher operating temperature of future nuclear reactors, weight loss due to thermal oxidation at different temperatures in addition to irradiation oxidation should also be incorporated in the future.

Acknowledgement

The authors would like to acknowledge the financial support of EPSRC through a joint project "Long Term Materials Behaviour and Chemistry - Fundamentals of Current and Future Uses of Nuclear Graphite" (EP/1002707/1)

References

[1] D.K.L. Tsang, B.J. Marsden. The development of a stress analysis code for nuclear graphite components in gas-cooled reactors. J of Nucl Mater. 350 (2006) 208-20.
[2] S. Li, S. Kyaw, A. Jones. Boundary conditions resulting from cylindrical and longitudinal periodicities Computers and Structures. Volume 133 (2014) Pages 122-30.
[3] Abaqus. User's Manual version 6.11 Dassault Systemes Simulia Corp. (2011).
[4] S. Kyaw, D. Tanner, A. Becker, W. Sun, D. Tsang. Modelling crack growth within graphite bricks due to irradiation and radiolytic oxidation. 20th European Conference on Fracture, Trondheim, Norway. (2014).
[5] G.B. Neighbour. Modelling of dimensional changes in irradiated nuclear graphites. J. Phys. D: Appl. Phys. . 33 (2000).
[6] E. D.Eason, G.N. Hall, B.J. Marsden, G. B. Heys. A model of Young's modulus for Gilsocarbon graphites irradiated in oxidising environments. Journal of Nuclear Materials, no. 436. (2013).
[7] G. Hall, B. Marsden, S. Fok. "The microstructural modelling of nuclear grade graphite" Journal of Nuclear Materials. 353 (2006) pp. 12-8.
[8] R. Moskovic, P. Heard, P. Flewitt, M. Wootton. "Overview of strength, crack propagation and fracture of nuclear reactormoderator graphite," Nuclear Engineering and Design. 263 (2013) pp. 431-42.
[9] D.K.L. Tsang, B.J. Marsden. The development of a stress analysis code for nuclear. Journal of Nuclear Materials. (2006) 208-20.
[10] L. Shi, H. Li, S.L. Fok, B.J. Marsden, S. Yu. The effect of softening on the predicted strength of brittle materials using a continuum damage mechanics failure model. 2nd International Topical Meeting on HIGH TEMPERATURE REACTOR TECHNOLOGY, Beijing, China, September 22-24, . (2004).
[11] E.D. Eason, G.N. Hall, B.J. Marsden, G.B. Heys. Models of bending strength for Gilsocarbon graphites irradiated in inert and oxidising environments. J. Nucl. Mater. . Volume 436 (2013) p. 208-16.
[12] P. Ouagne, G.B. Neighbour, B. McEnaney. Influence of oxidation on toughness parameters for two nuclear grade graphites. Journal of Physics D: Applied Physics. 38 (2005) 1259.
[13] B.T. Kelly, J.E. Brocklehurst. UKAEA Reactor Group studies of irradiation-induced creep in graphite. Journal of Nuclear Materials. 65 (1977) 79-85.
[14] B.T. Kelly, T.D. Burchell. The analysis of irradiation creep experiments on nuclear reactor graphite. Carbon. 32 (1994) 119-25.
[15] K. Tsang, B. Marsden. A simple mathematical model for isotropic nuclear graphite under irradiation condition. Int J of Appl Math and Mechs. 1 (2005) 1-19.
[16] Z. Zou, S.L. Fok, S.O. Oyadiji, B.J. Marsden. Failure predictions for nuclear graphite using a continuum damage mechanics model. Journal of Nuclear Materials. 324 (2004) 116-24.
[17] Z. Zou, S.L. Fok, B.J. Marsden, S.O. Oyadiji. Numerical simulation of strength test on graphite moderator bricks using a continuum damage mechanics model. Eng Fract Mech. 73 (2006) 318-30.
[18] S.T. KYAW, A.A. BECKER, W. SUN. AN OVERVIEW OF COHESIVE DAMAGE MODELS FOR SIMULATING CRACK GROWTH ENERGY OF NUCLEAR GRAPHITE. The 4th EDF Energy Nuclear Graphite Symposium. Engineering Challenges Associated with the Life of Graphite Reactor Cores, Nottingham, UK. (2014).
[19] J.M. Melenk, I. Babuska. Approximation with harmonic and generalized harmonic polynomials in the partition of unity method. Comput. Assist. Mech. Eng. Sci. 4 (1997) 607-32.